Appl Phys A
DOI 10.1007/s00339-012-7139-4

Applied Physics A
Materials Science & Processing

Molecular dynamics studies of ultrafast laser-induced nonthermal melting

Y. Wang · X. Xu

Received: 20 September 2011 / Accepted: 3 August 2012

Abstract Molecular Dynamics (MD) is employed to investigate nonthermal melting triggered by coherent phonon excitation in bismuth telluride, which has Peierls distortion in the lattice structure. Results showed that the structural distortion caused by coherent phonons appears as early as 80 fs, while it takes several picoseconds for the whole phonon-excited area to evolve into a liquid state. It was also found that the temperature in the phonon-excited area rises quickly within tens of femtoseconds, while the rest of the lattice remains at the initial temperature even after several picoseconds, which is separated from the high temperature region across a thin transition area. This phenomenon is analogous to the heat transfer across a solid–liquid interface, even though in our case there is no abrupt solid-liquid interface between the cold lattice and the quasiliquid.

1 Introduction

Nonthermal melting upon ultrafast laser excitation has been revealed in semiconductors [1–3], metals [4], and systems with Peierls distortion such as bismuth [5]. Nonthermal melting is distinguished from thermal melting in three aspects: (1) the liquid phase appears at sub-picosecond time scale, much faster than the time needed for the excited carrier to reach thermal equilibrium with the lattice [2–7], (2) it is typically observed at laser fluences much higher than the melting threshold [2, 3, 8], (3) it is hypothesized that the lattice might remain cold when the transition occurs [6]. Great efforts have been devoted to explain the ultrafast dynamics of excited carriers and the lattice in nonthermal melting [1, 2, 5, 7–10]. In semiconductors, experimental studies show that with a large percentage of excited carriers (above 5∼6 %), the potential energy surface is strongly modified and the antibonding of the conduction band accelerates the lattice disordering [1]. Furthermore, through computing the potential surface with dynamical simulations, Zijlstra and his colleagues concluded that ultrafast melting is triggered by a softening of transverse acoustic phonons and also found that the anharmonicity of the potential energy surface becomes important after about 100 fs at high excitation densities [11]. In bismuth, equilibrium positions of atoms are first displaced by the excited electron gas and then atoms start to oscillate around the new equilibrium positions along the direction of the Peierls distortion [12]. This process is called displacive excitation of coherent phonons (DECP), through which the longitudinal optical A_{1g} phonon mode is generated. Phonon oscillations can be observed through detecting the optical reflectivity change in ultrafast pump-probe experiments immediately following the femtosecond laser pulse [13, 14]. At this time scale, little energy has been transferred to the lattice through electron-phonon coupling; instead, atoms gain kinetic energy from an intensively modified potential surface [5]. This mechanical work exchange can lead to ultrafast disorder within a picosecond [5].

This study employs molecular dynamics (MD) to reveal the detailed phase change processes and mechanisms of ultrafast phase transition when coherent phonons are excited in bismuth telluride, which also has the Peierls distortion in the lattice structure. We attempt to investigate whether nonthermal melting can be triggered by coherent phonon generation, and the relevant phase change dynamics and temperature evolution compared with a normal thermal melting process.

Y. Wang · X. Xu (✉)
School of Mechanical Engineering and Birck Nanotechnology Center, Purdue University, West Lafayette, IN 47907, USA
e-mail: xxu@ecn.purdue.edu
Fax: +1-765-4940539

Published online: 25 August 2012

2 Numerical approach

As illustrated in Fig. 1, bulk Bi_2Te_3 has a rhombohedral primitive cell in the space group $R\bar{3}m$. At room temperature, the corresponding conventional cell is hexagonal with parameters $a = 4.369$ Å and $c = 30.42$ Å [15]. The hexagonal close-packed atomic structure consists of a periodic five-fold layer along the c-axis: Te I–Bi–Te II–Bi–Te I. The bonding force is covalent within the five-fold layers and Van der Waals between the layers [16]. The nearest-neighbor distances between atoms in different monatomic layers are 3.04 Å for the Te I–Bi bond, 3.24 Å for the Te II–Bi bond, and 3.72 Å for the Te I–Te I bond [16].

Huang and Kaviany developed a set of three-body interatomic potentials for bulk Bi_2Te_3 [17]. Even though the properties predicted by this set of 24-parameter potentials agree well with experimental results, the computation cost of MD using a three-body potential can be very high. Qiu and Ruan developed a set of two-body potentials from the density-functional theory (DFT) and implemented into MD simulations to predict the lattice thermal conductivity of bulk Bi_2Te_3 [15]. Their predicted lattice thermal conductivities agree with experimental results within the temperature range from 150 to 500 K. The fitted two-body potentials take the form:

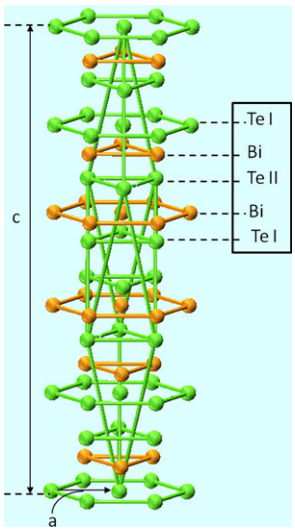

Fig. 1 The crystal structure of Bi_2Te_3, where both rhombohedral and conventional hexagonal unit cells are delineated

$$U_{ij} = U_{ij}^{s} + \frac{q_i q_j}{r_{ij}} = D_e\left\{\left[1 - \exp\left[-a(r_{ij} - r_0)\right]\right]^2\right\} + \frac{q_i q_j}{r_{ij}} \quad (1)$$

Here, the short-range potential takes the Morse form, where D_e corresponds to the depth of potential well, r_0 denotes the equilibrium bond distance, and a is the bond elasticity. Only the nearest-neighbor interactions are considered. q_i and q_j in the last term are the effective charges of the ions. The charge values are 0.38, −0.26, and −0.24 for Bi, Te I, and Te II, respectively.

In this study, the two-body potentials are adopted. To evaluate the long-range Coulomb interaction effectively, Wolf's summation [18] is applied with a cut-off radius of 11.28 Å. The parameters for the Morse potentials are listed in Table 1.

In the MD simulation, coherent phonons are excited in the following way: the two pairs of Bi and Te I atoms are stretched from the center (Te II) along the c-axis, and then the atoms are released. This is to imitate the displacement from the atomic equilibrium positions due to photon-dipole interaction when A_{1g} phonons are excited by ultrafast laser pulses. Frequency of A_{1g} phonons calculated using this method is 1.83 THz, which is only about 3 % lower than that measured with ultrafast pump-probe experiments (1.86 THz) [13].

3 Results and discussion

In order to compare the phase change phenomena with and without coherent phonon excitation, simulations of two cases are conducted on a 27 nm-thick Bi_2Te_3 thin film. The lateral dimension is about 1.3 × 1.3 nm, with the period boundary condition applied. We assume the laser pulse is a delta function. In the first case, the energy from the laser pulse is treated as a heating source. All the laser energy is absorbed by electrons at time $t = 0$, and then the energy deposited into electrons is transferred to the lattice exponentially. At time t, the laser energy absorbed between z and $z + \Delta z$ can be expressed as

Table 1 Parameters of the Morse potential

Bond	D_e (eV)	a (1/Å)	r_0 (Å)	r_c (Å)
Bi–Bi	0.085	2.212	4.203	5.5
Bi–Te I	0.975	1.285	3.089	4.0
Bi–Te II	0.582	1.257	3.251	4.0
Te I–Te I	0.076	1.675	3.642	5.0
Te I–Te II	0.807	0.731	4.497	5.5
Te II–Te II	0.066	2.876	4.312	5.0

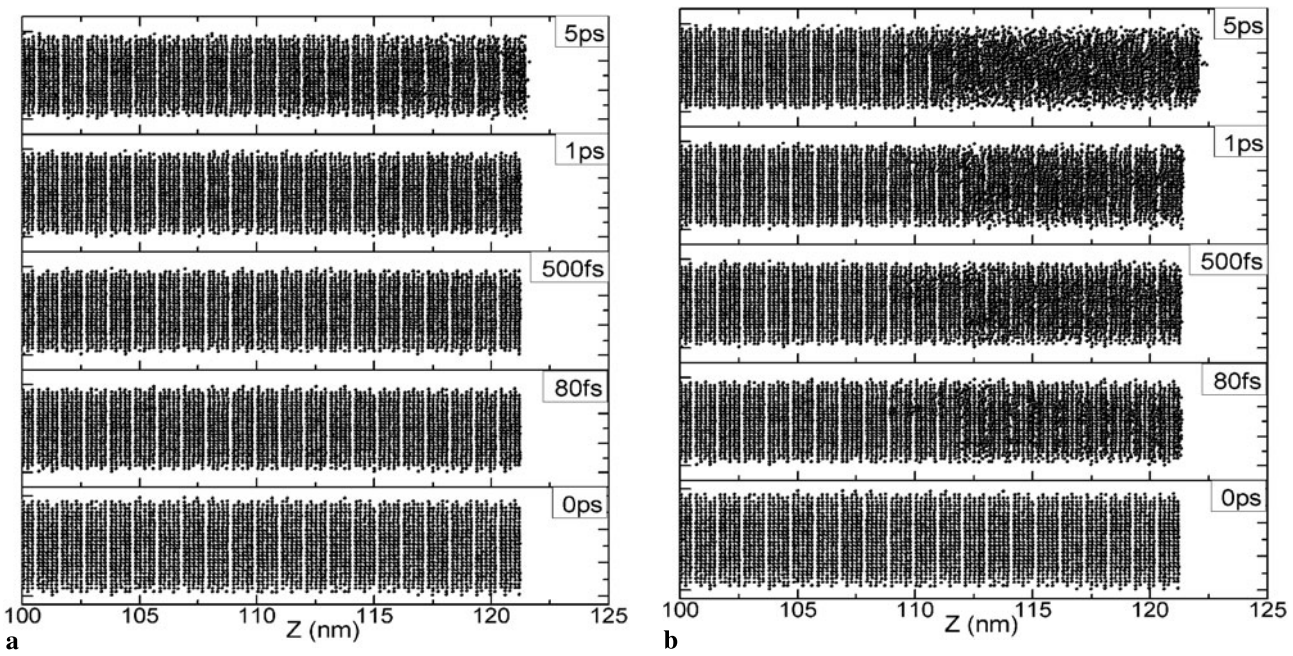

Fig. 2 Snapshots of atomic distributions of (**a**) laser heating with absorbed laser fluence of 13.1 J/m^2 and (**b**) nonthermal melting triggered by coherent phonon excitation, corresponding to absorbed fluence 13.1 J/m^2

$$\Delta E = AF\frac{\Delta t}{\tau}\exp(-t/\tau)\left[\exp(-z/\delta) - \exp\left(-(z+\Delta z)/\delta\right)\right] \tag{2}$$

where A is the illuminated area, F is the absorbed laser fluence, and Δt is the time step in MD. τ is the time constant of energy transfer (5 ps used in the calculation) and δ is the absorption depth (10 nm at the laser wavelength of 400 nm). In the calculation, the absorbed laser energy is deposited into the lattice through scaling the velocity with a factor $S = \sqrt{1 + \Delta E/E_k}$, where E_k is the kinetic energy of atoms within the layer from z to $z + \Delta z$. The absorbed laser fluence used in the calculation is 13.1 J/m^2.

In the second case, coherent A_{1g}^1 phonons are excited within the top 10 nm layer, and are randomly distributed. The amount of energy deposited into coherent phonons is the same as that in the first case.

Figure 2 illustrates the snapshots and temperature distributions of both cases. In the case of normal thermal heating, thermal distortion appears around 5 ps (Fig. 2a). A continuous temperature gradient is established across the whole film throughout the time of consideration. The surface temperature at 5 ps is around 2,000 K, much higher than the melting temperature (858 K [19]), and the structure remains as solid. This phenomenon is called super heating, which has been observed in a wide variety of solids during ultrafast heating [20, 21]. The liquid phase starts to nucleate at the surface around 5 ps, then the liquid-solid interface moves into the sample, which is typical for thermal melting. For the second case with coherent phonon generation, structure distortion starts as early as 80 fs (Fig. 2b)), scattered at isolated locations. Around 500 fs, the distortion develops into larger areas and localized liquid-like structure starts to appear. Here, both the distortions caused by coherent phonons and from the raised temperature contribute to the formation of the localized liquid-like structure, since part of the energy deposited into the coherent phonons is converted to the kinetic energy of atoms. However, we call this phenomena "nonthermal" melting in order to distinguish it from the pure heating situation. An interesting phenomenon was observed here: the liquid phase was first developed within each five-fold layer, and then the distortion crosses layers, and sweeps the whole phonon-excited area. This feature might be unique to Bi_2Te_3, where there are different bonding forces within (covalent) and between (Van der Waals) unit cells. A complete transition to liquid takes several picoseconds. We call the mixed phase before transition to liquid a "quasi-liquid" phase.

Another observation is that the lattice underneath the phonon-excited area is almost undisturbed during nonthermal melting. This indicates that the heat conduction from phonon-excited area to the cold lattice is greatly suppressed. From the temperature profile, Fig. 3b, the temperature steps from around 2,000 K to 300 K across a region of about 5 nm thick. The temperature below this 5 nm-thick region remains around 300 K even at around 5 ps, which is very different from the pure heating case. The highest surface temperatures in the two cases are almost identical. Similar phenomenon is observed in the ultrafast laser melting of silver [22]. It

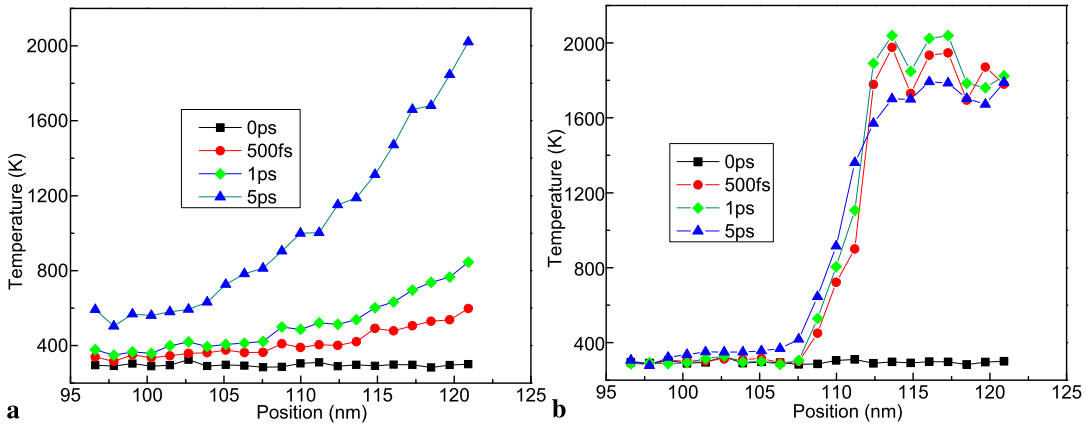

Fig. 3 Temperature distribution in Bi_2Te_3 thin film. (**a**) Laser heating with absorbed laser fluence of 13 J/m^2 and (**b**) nonthermal melting triggered by coherent phonon excitation, corresponding to absorbed fluence 13 J/m^2

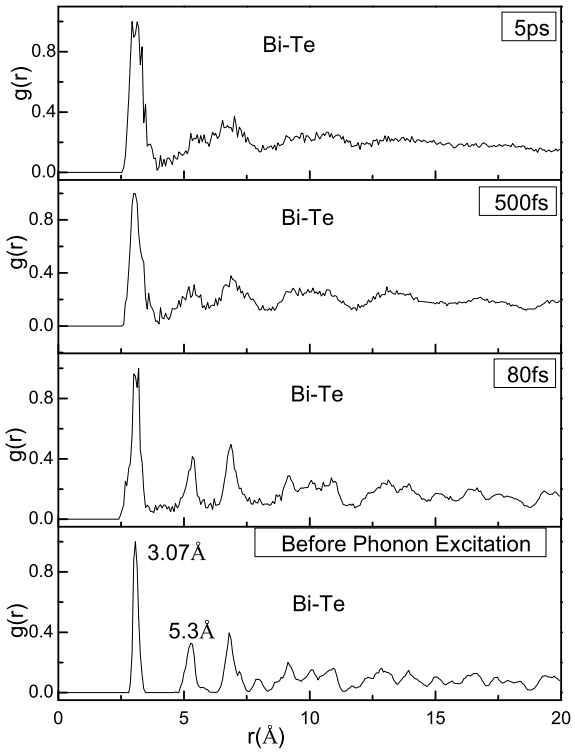

Fig. 4 Radial distribution functions of the Bi–Te bond at different time after laser irradiation

was found from the experiment that only a thin surface layer undergoes melting during the first several picoseconds. The melting front propagates into the sample with a very low velocity and the surface temperature remains above the melting temperature for 20∼30 ps. The reason for limited heat conduction from the melted surface area is attributed to the weak electron-phonon coupling [22]. On the other hand, this cold-lattice picture was not consistent with the ab-initio MD study of silicon [23]. In this study, no electronic effect is considered. Therefore, the weak electron-phonon coupling could not explain the ineffective heat transfer between the phonon-excited area and the cold lattice. In our results, the difference in the temperatures between the area where laser energy is deposited and the lattice below is caused by the effective transfer of energy from photons to the coherent phonons.

Radial distribution function (RDF) [24] can help to understand different stages in non-thermal melting, which is defined as

$$g(r_{\alpha\beta}) = \frac{V}{N}\frac{n_{r_{\alpha\beta}\to r_{\alpha\beta}+dr_{\alpha\beta}}}{4\pi r_{\alpha\beta}^2 dr_{\alpha\beta}} \tag{3}$$

where V represents the volume of the computation domain, N is the total number of atoms, and α and β denote two different types of atoms. $n_{r_{\alpha\beta}\to r_{\alpha\beta}+dr_{\alpha\beta}}$ is the number of pairs of $\alpha\beta$ atoms within the spherical shell between radius $r_{\alpha\beta}$ and $r_{\alpha\beta}+dr_{\alpha\beta}$. For laser heating with coherent phonon generation, RDFs of Bi–Te bonds are calculated at a number of time steps and plotted in Fig. 4. Before laser heating (time 0), spikes in the RDF denote short-range and long-range orders in crystalline Bi_2Te_3. The first two peaks in the RDFs represent the distance between the Bi atoms and their nearest Te I neighbors (3.07 Å) and next-nearest Te I neighbors (5.3 Å) within the fivefold layer. At around 80 fs, the lattice structures are only disturbed slightly. At around 500 fs, peaks are blurred and shifted at small r (short-range structures) and decay at larger r, indicating that the long-range orders start to be destroyed. From 500 fs to 5 ps, long-range structures gradually disappear together with some short-range structures. Only the first few peaks are still shown in RDFs around 5 ps, which is typical for pure liquid phases.

From the analyses above, it can be seen that the phenomena occurring during ultrafast laser excitation of coherent phonons are drastically different from a normal melting process. There can be a short time period where nonthermal melting can occur, before the entire laser heated area becomes liquid.

4 Conclusion

In summary, ultrafast nonthermal melting triggered by coherent phonon excitation is simulated using MD and compared with normal thermal melting. The calculation results reveal the details of how nonthermal phase transitions occur after coherent phonon excitation. It is found that long-range orders begin to be destroyed within 500 fs after the laser pulse, and these distortions are scattered throughout the photo-excited layer. For Bi_2Te_3, this scattered distortions then first spread within the unit cell, then cross the boundaries between unit cells. The transition from this "quasi-liquid" state to liquid takes several picoseconds. The melted layer reaches a temperature above the equilibrium melting temperature, while the lattice underneath it remains cold.

Acknowledgements Support to this work by the Air Force Office of Scientific Research (AFOSR) (FA9550-08-1-0091) and the National Science Foundation (0933559) are gratefully acknowledged.

References

1. A. Rousse, C. Rischel, S. Fourmaux, I. Uschmann, S. Sebban, G. Grillon, Ph. Balcou, E. Förster, J.P. Geindre, P. Audebert, J.C. Gauthier, D. Hulin, Nature **410**, 65 (2001)
2. C.W. Siders, A. Cavalleri, K. Sokolowski-Tinten, Cs. Toth, T. Guo, M. Kammler, M. Horn von Hoegen, K.R. Wilson, D. von der Linde, C.P.J. Barty, Science **286**, 1340 (1999)
3. C.V. Shank, R. Yen, C. Hirlimann, Phys. Rev. Lett. **51**, 900 (1983)
4. C. Guo, G. Rodriguez, A. Lobad, A.J. Taylor, Phys. Rev. Lett. **84**, 4493 (2000)
5. G. Sciaini, M. Harb, S.G. Kruglik, T. Payer, C.T. Hebeisen, F.J.M. Heringdorf, M. Yamaguchi, M.H. Hoegen, R. Ernstorfer, R.J.D. Miller, Nature **458**, 56 (2009)
6. S.K. Sundaram, E. Mazur, Nat. Mater. **767**, 217 (2002)
7. P.B. Hillyard, K.J. Gaffney, A.M. Lindenberg, S. Engemann, R.A. Akre, J. Arthur, C. Blome, P.H. Bucksbaum, A.L. Cavalieri, A. Deb, R.W. Falcone, D.M. Fritz, P.H. Fuoss, J. Hajdu, P. Krejcik, J. Larsson, S.H. Lee, D.A. Meyer, A.J. Nelson, R. Pahl, D.A. Reis, J. Rudati, D.P. Siddons, K. Sokolowski-Tinten, D. von der Linde, J.B. Hastings, Phys. Rev. Lett. **98**, 125501 (2007)
8. A.M. Lindenberg, J. Larsson, K. Sokolowski-Tinten, K.J. Gaffney, C. Blome, O. Synnergren, J. Sheppard, C. Caleman, A.G. MacPhee, D. Weinstein, D.P. Lowney, T.K. Allison, T. Matthews, R.W. Falcone, A.L. Cavalieri, D.M. Fritz, S.H. Lee, P.H. Bucksbaum, D.A. Reis, J. Rudati, P.H. Fuoss, C.C. Kao, D.P. Siddons, R. Pahl, J. Als-Nielsen, S. Duesterer, R. Ischebeck, H. Schlarb, H. Schulte-Schrepping, T. Tschentscher, J. Schneider, D. von der Linde, O. Hignette, F. Sette, H.N. Chapman, R.W. Lee, T.N. Hansen, S. Techert, J.S. Wark, M. Bergh, G. Huldt, D. van der Spoel, N. Timneanu, J. Hajdu, R.A. Akre, E. Bong, P. Krejcik, J. Arthur, S. Brennan, K. Luening, J.B. Hastings, Science **308**, 392 (2005)
9. D.M. Fritz, D.A. Reis, B. Adams, R.A. Akre, J. Arthur, C. Blome, P.H. Bucksbaum, A.L. Cavalieri, S. Engemann, S. Fahy, R.W. Falcone, P.H. Fuoss, K.J. Gaffney, M.J. George, J. Hajdu, M.P. Hertlein, P.B. Hillyard, M. Horn-von Hoegen, M. Kammler, J. Kaspar, R. Kienberger, P. Krejcik, S.H. Lee, A.M. Lindenberg, B. McFarland, D. Meyer, T. Montagne, E.D. Murray, A.J. Nelson, M. Nicoul, R. Pahl, J. Rudati, H. Schlarb, D.P. Siddons, K. Sokolowski-Tinten, Th. Tschentscher, D. von der Linde, J.B. Hastings, Science **315**, 633 (2007)
10. K. Sokolowski-Tinten, C. Blome, J. Blums, A. Cavalleri, C. Dietrich, A. Tarasevitch, I. Uschmann, E. Forster, M. Kammler, M. Horn-von-Hoegen, D. von der Linde, Nature **422**, 287 (2003)
11. E.S. Zijlstra, J. Walkenhorst, M.E. Garcia, Phys. Rev. Lett. **101**, 135701 (2008)
12. T.K. Cheng, S.D. Brorson, A.S. Kazeroonian, J.S. Moodera, G. Dresselhaus, M.S. Dresselhaus, E.P. Ippen, Appl. Phys. Lett. **57**, 1004 (1990)
13. Y. Wang, X. Xu, R. Venkatasubramanian, Appl. Phys. Lett. **93**, 113114 (2008)
14. C.M. Liebig, Y. Wang, X. Xu, Opt. Express **18**, 20498 (2010)
15. B. Qiu, X. Ruan, Phys. Rev. B **80**, 165203 (2009)
16. W. Richter, H. Kohler, C.R. Becker, Phys. Status Solidi B **84**, 619 (1977)
17. B.L. Huang, M. Kaviany, Phys. Rev. B **77**, 125209 (2008)
18. D. Wolf, P. Keblinski, S.R. Phillpot, J. Eggebrecht, J. Chem. Phys. **110**, 8254 (1999)
19. A.F. Gibson, R.E. Burgess (eds.), *Progress in Semiconductors* (Wiley, New York, 1963)
20. X. Xu, C.P. Grigoropoulos, R.E. Russo, J. Heat Transf. **117**, 708 (1995)
21. X. Xu, G. Chen, K.H. Song, Int. J. Heat Mass Transf. **42**, 1371 (1999)
22. W.L. Chan, R.S. Averback, D.G. Cahill, A. Lagoutchev, Phys. Rev. B **78**, 214107 (2008)
23. P.L. Silvestrelli, A. Aavi, M. Parrinello, D. Frenkel, Phys. Rev. Lett. **77**, 3149 (1996)
24. M.P. Allen, D.J. Tildesley, *Computer Simulation of Liquids* (Clarendon/Oxford University Press, Oxford/New York, 1987)